Materials at High Temperatures, Volume 35, 2018 - Issue 1-3: Microscopy of Oxidation 10, pp151-158
DOI:10.1080/09603409.2017.1389100

Corrosion fatigue testing: the combined effect of stress and high temperature corrosion

Neil Chapman[1 and 2], Laurie Brooking[2], Joy Sumner[2], Simon Gray[2] and John Nicholls[2]

[1] Siemens Industrial Turbomachinery Ltd, Ruston House, PO Box 1, Waterside South, Lincoln, LN5 7FD

[2] Cranfield University, College Road, Cranfield, MK43 0AL

Abstract

A corrosive environment can have a detrimental effect on the fatigue life of a material due to a change in failure mechanism. Attempts have been made to replicate this change on nickel-base superalloy CMSX-4 cast in the <001> orientation. Fatigue testing in air, of this material typically produces a fracture on an angle of approximately 55° which is consistent with the fracture having propagated on a {111} slip plane. The aim of the research was to fatigue test in a corrosive environment with the purpose of producing a crack/fracture which deviated from the typical angle and thus confirm that the corrosive environment had affected the fatigue mechanism. It was concluded that the change in mechanism to high temperature corrosion fatigue was associated with a reduced load application rate together with precorroding the test specimens to trigger the initiation of the corrosion fatigue mechanism.

Keywords: corrosion fatigue, waveform, load application rate, precorrosion

1.0 Introduction

Materials which are used in rotating parts of industrial gas turbines (IGTs) are subjected to harsh operating conditions which include high stresses and temperatures. In addition, an IGT may operate in a number of different atmospheres such as: industrial, marine or rural, all of which are likely to contain different impurities in the air that may cause corrosion issues[1].

Nickel-base superalloys are routinely used in IGTs due to their high temperature mechanical properties[1,2] and their development has included improvements in their resistance to corrosion attack. This has been achieved by including chromium and

Published by Taylor & Francis. This is the Author Accepted Manuscript issued with:
Creative Commons Attribution Non-Commercial License (CC:BY:NC 4.0).
The final published version (version of record) is available online at DOI:10.1080/09603409.2017.1389100
Please refer to any applicable publisher terms of use.

aluminium in the chemistries with the purpose of growing either a protective chromia or alumina scale. The superalloys may therefore be classed as either a chromia or an alumina former[1,2], depending on the alloy composition.

Chromia formers tend to be used at temperatures below 900°C due to chromia forming volatile species above this temperature, whilst alumina formers are used above 900°C since less protective scales are formed below this temperature[1]. IGT components though do not generally experience a uniform temperature and different sections of the same component may experience temperatures above and below 900°C. The nickel-base superalloy CMSX-4 is an alumina former[1] and thermal exposure tests on this material, conducted at 700°C, revealed the primary scale observed was a thin aluminium rich layer. Due to the instability of the protective alpha alumina phase at this temperature, the scale was attributed as being either a less protective transient Al_2O_3 phase or a mixed oxide of Al/Cr [3].

Nickel-base superalloys, even when they have grown a protective scale, are not immune to corrosion attack though and under certain conditions the attack may result in high rates of material loss. One form of corrosion that can result in pitting and rapid material loss is type II hot corrosion[1,2-3]. This form of corrosion tends to occur between the temperatures of 600 to 800°C[1] and requires the presence of deposits such as sulphates and SO_3[1,2], within the gas phase.

There are two stages to type II hot corrosion: incubation and propagation. Once the attack has penetrated any protective scale (considered the end of the incubation stage), the attack will enter the propagation stage of corrosion and the superalloy itself will be attacked resulting in high rates of material loss[3]. These rates though, may alter with exposure time as was found from type II hot corrosion tests that were performed on CMSX-4 material[3]. During these tests, the propagation rates fell with exposure time which was thought to be most likely due to thick deposits/corrosion product scale that had formed inhibiting the supply of the corrosive species to the material/scale interface[3].

Any reduction in cross section caused by the corrosion attack will effectively increase the stresses acting on the IGT components and the rate of loading/straining may also have an effect on the fatigue life of the material. Classically, a series of fatigue tests are performed to evaluate an S-N curve which can be used to determine the

fatigue life of a material for a specific set of conditions such as: temperature, environment and R-ratio. Figure 1 shows an example of an S-N curve which may be made up of up to three different regions. In region I, the tests are performed at stresses at or above the materials' yield strength and hence the material behaves in an elasto-plastic manner. In region II, the material is stressed below the yield strength and so behaves in an elastic manner. Region III defines an unlimited life but materials with a face centred cubic structure, such as nickel, do not seem to experience this region[4].

Fatigue tests may be performed in strain or load control and generally, strain control is used for the elasto-plastic region of fatigue testing where the associated strain is the summation of elastic and plastic strains. Load control tends to be used in the elastic region of fatigue testing where a one-to-one correspondence between stress and strain exists. It is therefore unimportant whether fatigue testing in the elastic region is conducted using strain or load control[4].

For a given total strain, reducing the strain rate may result in shorter fatigue lives when the tests are conducted in the elasto-plastic region of fatigue testing. This effect was observed on tests performed at elevated temperatures on nickel-base alloy 718 in air[5]. The tests were also performed with only elastic loading which gave no noticeable interaction between life and strain rate[5]. The most likely cause is an interaction between creep and fatigue at the elevated temperatures, however, no hypothesis was ventured by the author[5] as to a possible mechanism that may be responsible for this behaviour.

A molecular dynamic simulation of monocrystalline nickel indicated the strain rate effect may be explained by a mechanism involving microstructural changes in the form of dislocations being generated at the crack tip at temperature. The simulations showed that when a set strain level was reached with different strain rates, the faster strain rates produced slower growing cracks that tended to propagate in a ductile manner with dislocations generated at the crack tip. This had the effect of blunting the crack tip and produced relatively low peak stress levels at the tip of the crack. The slower strain rates though produced faster propagating cracks which behaved in a more brittle manner and induced fewer dislocations at the crack tip resulting in greater peak stress values at the tip of the crack[6]. These peak stress values are

highly localised and upon repeated cycling, form micro-cracks and a plastic zone ahead of the advancing crack tip[7].

During the growth of a corrosion fatigue crack, it is reported that it is necessary for the corrosive compound to be supplied to the crack tip, interact with newly exposed crack surface by adsorption and diffusion, and finally the reacted products on the crack surfaces need to be removed in order to prevent a build up at the crack tip which may influence local stresses[8]. An important factor then, is the rate at which the corrosive compound reaches the crack tip and slowing down the frequency of the fatigue testing should allow more time for this to happen. It has also been commented that frequencies below 1 Hz have the greatest environmental effect on the fatigue properties of nickel-based superalloys[9].

Slowing the frequency of the fatigue tests down can be achieved by increasing the duration of the entire selected waveform or selected periods of the waveform which include the stress or strain (depending on whether the fatigue test is performed in load or strain control) application time, the maximum stress/strain hold time, the stress/strain decreasing time and the minimum stress/strain hold. Fatigue tests, performed on a low carbon alloy steel in an aqueous solution of 3% NaCl at a temperature of 25°C, led to the conclusion that of all the periods of a waveform, lengthening the stress application period up to 10 seconds had the greatest environmental effect and was attributed to corrosive dissolution on fresh crack surfaces that were formed during that period of the waveform[10]. One premise to be examined is whether this observation applies to high temperature corrosion fatigue.

The aim of the current work was to perform corrosion fatigue tests in service like-type II hot corrosion conditions on the face centred cubic single crystal nickel-based superalloy CMSX-4 that had been cast in the <001> orientation. The purpose of the corrosion fatigue tests was to establish parameters that would allow sufficient time for the corrosive compounds to affect the fatigue mechanism. The parameters under evaluation were the various periods of a trapezoidal waveform (Figure 2) and whether or not to precorrode the test specimens. Typically, fatigue tests conducted in air on this material and orientation produce fracture surfaces on approximate angles of 55° which is consistent with the fracture having propagated on a {111} slip plane.

Deviation from this typical angle would therefore be strongly suggestive that the environment had affected the fatigue mechanism of the material.

2.0 Experimental methods

The material under investigation was the superalloy CMSX-4 that had been solution treated and precipitation hardened but had not been hot isostatic pressed. The nominal composition of this superalloy is shown in table 1. After casting, this material typically contains significant segregation, γ/γ' eutectic regions and pores[11]. The solution heat treatment is therefore carried out in order to achieve a balanced chemical composition and dissolve the eutectic regions but this is at the expense of increased levels of porosity[11]. The precipitation hardening then provides the material with the desirable mechanical properties which makes it suitable for use as IGT components.

Plain fatigue test specimens with a gauge diameter of 6 mm (Figure 3) were machined from bars that were cast in the <001> orientation and tested on an axial fatigue testing machine in load control at a temperature of 550°C. Due to the flexibility in controlling the various periods of applying the load, the trapezoidal waveform was selected. This waveform is expressed in terms of the duration of each respective period. For example, a 1-1-1-1 s waveform describes a 1 second load increasing period with1 second at maximum load hold followed by 1 second with the load decreasing and finally 1 second at the minimum load hold period.

The fatigue testing atmosphere was either laboratory air or 300 ppm SO_2 in air (flow rate between 25 and 50 SCCM, preheated to the test temperature). The test specimens were loaded into the fatigue machine in such a manner so that they sat within a gas sheath within the induction coil that was used for attaining the test temperature. The gas sheath ensured the corrosive gas used in the corrosion fatigue tests, flowed over the surfaces of the test specimen. The tests were only started after the test temperature had been achieved and left for 15 minutes to ensure the temperature had equalised throughout the cross section of the test specimen. Type K thermocouples were used for measuring the test temperature.

The maximum and minimum stress levels used were the same for all of the fatigue and corrosion fatigue tests which were 800 and 0 MPa respectively. This ensured

that all the tests were conducted in the elastic region of fatigue testing. Table 2 summarises the conditions of the fatigue tests conducted.

The fatigue testing performed in laboratory air included the waveforms: 1-1-1-1 and 10-1-1-1 s. No salts were applied to either of these test specimens. These can be considered as baseline tests.

Corrosion fatigue testing performed in the SO_x environment on non-precorroded test specimens included the waveforms: 1-1-1-1, 10-1-1-1 and 1-10-1-1 s. For these tests, the test specimens were sprayed evenly around the surfaces between the threads with 0.114 mg cm^{-2} with an 80/20 mol% mix of $(Na/K)_2SO_4$ salt deposits before the testing began. Applying a specific quantity of salt though, implies that the flux may vary for the different corrosion fatigue tests depending on when the test specimen fails. The method for applying the salts, which were dissolved in water, involved heating the specimens up to approximately 200°C after which the salts were sprayed onto the hot surfaces. The heat caused the water to flash evaporate leaving the salts on the sprayed surfaces. If a corrosion fatigue test completed 100 hours without failing, the test was stopped and a further 0.114 mg cm^{-2} of salt was applied before the test was re-started.

The corrosion fatigue testing performed in the SO_x environment on precorroded test specimens included the waveforms: 1-1-1-1 and 10-1-1-1 s. The precorrosion of these test specimens involved evenly spraying the 80/20 mol% mix of $(Na/K)_2SO_4$ salts onto the surfaces between the threads, using the same methodology as described previously, with a flux rate of 5 µg cm^{-2} h^{-1}. That is, the salts were sprayed after 0, 100, 200, 300 and 400 hours of thermal exposure, at the same temperature as the fatigue tests, and the total duration of the thermal exposures were 500 hours. If any corrosion fatigue test using the precorroded test specimens completed 100 hours without failing, the test was stopped and a further 0.114 mg cm^{-2} of salt deposits was applied before the test was re-started.

A fatigue test in laboratory air using a 10-1-1-1 s waveform was also performed on a precorroded test specimen that had all of the salts washed off. The purpose of this test was to determine whether corrosion pitting alone was enough to alter the fatigue mechanism or if the corrosive salts and environment were required throughout the test.

As part of an initial test program to identify parameters which affected the fatigue mechanism, only one test was conducted for each test condition with the exception of the corrosion fatigue test conducted with a 1-10-1-1 s waveform and a non-precorroded specimen. A repeat of this test was performed.

The number of tests conducted is acknowledged as being small and the cycles to failure data would be subject to any potential scatter involved. For this reason, the cycles to failure data was not used for assessing whether the fatigue mechanism had been affected but is included in this article in a normalised form for reference purposes only (Table 3). Instead, the assessment was based on visual observations of the crack/fracture paths/angles. These visual observations were conducted with the naked eye, a low powered optical microscope and an SEM. Of particular interest was whether any of the test conditions had produced crack surfaces which deviated away from the typical 55° angle. If cracks had deviated away from this angle, EDX analysis using a series of rectangular region X-ray acquisitions on the crack surface was performed to determine which corrosive element(s) had contributed to the deviation. Microsections were then taken and the resulting cross sections viewed using a high powered optical microscope and SEM.

3.0 Results and discussion

Table 3 shows a summary of the fatigue and corrosion fatigue tests which did and did not result in a crack/fracture that deviated from the 55° angle.

Both of the non-precorroded test specimens that were fatigue tested in laboratory air showed crack/fracture features on angles of approximately 55°. This crack/fracture angle is shown in figure 4 which was produced using the 10-1-1-1 s waveform. This is consistent with typical results and indicates that the different stress application rates of 800 MPa s^{-1} and 80 MPa s^{-1}, associated with the respective 1-1-1-1 and 10-1-1-1 s waveforms could not be wholly responsible for any crack/fracture deviation that was subsequently found on the corrosion fatigue test specimens.

The non-precorroded test specimens that were subjected to the corrosion fatigue tests using the 1-1-1-1 and 1-10-1-1 s waveforms, also produced fracture facets that were only on approximate angles of 55°. A repeat of 1-10-1-1 s test was performed and exceeded the duration of the original test by a factor of 1.5 without failing. The

repeat test was therefore considered a runout and did not provide any data regarding crack/fracture angles. However, the non-precorroded corrosion fatigue test using the 10-1-1-1 s waveform produced a crack that was initially flat and perpendicular to the surface of the specimen before transitioning to the 55° angle (Figure 5). The perpendicular crack, which was in the shape of a thumbnail with approximate maximum width and depth dimensions of 2.0 and 1.5 mm respectively, also exhibited beach marks (Figure 6) which were suggestive that the crack was growing as a start-stop-start event. EDX analysis (Figure 7a and 7b) of the crack surface indicated sulphur was the main element present, in decreasing amounts, from the surface of the test specimen to the tip of the perpendicular crack. Small quantities of sodium were also present and again displayed a generally decreasing trend from the surface to the perpendicular crack tip. Potassium though was only present in trace amounts. After the EDX analysis, the test specimen was sectioned and this revealed the corrosion product on the perpendicular crack was very thin with an approximate thickness of 0.2 μm at the mid crack position (Figure 8). These corrosion fatigue tests have indicated, based on the 10-1-1-1 and 1-10-1-1s waveforms which have the same frequency, that frequency or the maximum load hold time are not prime factors which allow the environment time to affect the fatigue mechanism. Instead, the load application rate appears to be of greater importance and lowering this has the effect of decreasing the frequency providing the other periods of the waveform remain constant.

Precorroding the test specimens before conducting the corrosion fatigue tests with the 1-1-1-1 and 10-1-1-1 s waveforms also produced initial flat thumbnail shaped perpendicular cracks that exhibited beach marks before transitioning to an approximate 55° angle. EDX analysis of the 10-1-1-1 s crack (Figure 7c and 7d) showed a similar pattern to that observed on the non-precorroded test specimen used on the corrosion fatigue 10-1-1-1 s test in that sulphur and sodium were present in decreasing amounts from the surface of the specimen to the crack tip with the main element being sulphur. The approximate maximum width and depth dimensions of the perpendicular crack for the precorroded 1-1-1-1 s corrosion fatigue test were measured at 1.0 and 0.9 mm respectively. The width and depth dimensions of the initial perpendicular crack on the precorroded 10-1-1-1 s corrosion fatigue test specimen were 3.6 and 2.0 mm respectively. It was also observed that

the precorroded 10-1-1-1 s corrosion fatigue initial perpendicular crack differed from the other perpendicular cracks in that it had propagated on two separate crack planes and subsequently joined together (Figure 9). All other perpendicular cracks had only propagated on a single crack plane. For both of the corrosion fatigue tests using precorroded test specimens, the size of the flat perpendicular cracks had increased when compared to the non-precorroded corrosion fatigue counterparts. Since the tests were performed at temperatures at which a protective alumina scale does not form, the propagation stage of corrosion would have started relatively early. The importance of precorroding the specimens was therefore to diffuse the corrosive species into the material before the fatigue testing started.

The precorroded test specimen that had all of the salt deposits washed off and then tested in air using a 10-1-1-1 s waveform, exceeded the duration of the precorroded corrosion fatigue counterpart by a factor of 5 without failing. This test was considered a runout and indicated that the salt deposits and SO_x environment were of greater significance than any potential corrosion pitting that may have occurred during the initial precorrosion phase.

SEM analysis of the initial flat perpendicular corrosion fatigue cracks found on the precorroded and non-precorroded test specimens, suggested propagation could initiate and occurred from internal pores (Figure 10) as well as surface breaking corrosion pits. Un-etched microsections (Figure 11) confirmed the initial flat cracks were approximately 90° to the surface of the test specimens and after electrolytically etching in a solution of: 20 mls hydrofluoric acid, 40 mls of glycerol and 340 mls of water, the internal pores appeared to be associated with eutectic regions (Figure 12).

The results obtained suggest that the internal pores associated with eutectic regions within the material were prime sites for the initiation of corrosion fatigue cracks. These pores may have acted as stress raisers in a material that was likely to have been affected by the diffusion of the corrosive species. Once a crack had initiated, low rates of application of stresses during the fatigue cycling may have resulted in fewer dislocations generated at the crack tip and thus minimised any possible crack tip blunting. In turn, the localised peak stresses associated with the sharper cracks may have caused a relatively large plastic zone ahead of the crack tip containing high vacancy concentrations within the associated slip bands[9], along with a greater

concentration of micro-cracks[7]. This would provide short circuit diffusion paths allowing a relatively fast diffusion of the corrosive species (believed to be sulphur). Additionally, the beach marks observed are suggestive that the corrosion fatigue cracking was a start-stop-start process. This would be possible if the rate of crack propagation was greater than the rate of corrosive diffusion. That is, once a crack tip had caught up with the diffusion front, the crack would have stopped propagating if the remaining cross sectional area of the test specimen could support the load. The corrosive diffusion though would continue and when the material ahead of the crack tip had been sufficiently affected, the crack would start to propagate again until it once again caught up with the diffusion front. If the size of the remaining cross section of the test specimen was insufficient to support the load, the crack would begin to propagate every cycle until final fracture occurred. Under this condition, and without the influence of the environment, the crack growth transitioned back to the 55° classic slip band angle for this alloy system.

In summary, the factors which appeared to have affected the typical air fatigue mechanism the most under the corrosive test conditions used were the load application rate and precorrosion of the test specimens. The observation that the load application rate had affected the mechanism was in agreement with the findings, albeit based on different materials, corrosive conditions and temperature of testing, from Ref. 10, which concluded that this was due to the dissolution of the corrosive species on the freshly exposed crack surfaces formed under the load application period. The molecular dynamic simulations performed in Ref. 6 though, indicate that the change in mechanism may also be associated with the lack of crack tip blunting associated with low strain rates.

4.0 Conclusion

The parameters that affected the typical air fatigue mechanism of solution treated and precipitation hardened CMSX-4 material cast in the <001> orientation the most, when tested under the corrosive conditions, were the 10-1-1-1 s waveform and precorrosion of the test specimens. It is postulated that with stress application rates as low as 80 MPa s^{-1}, significant crack tip blunting by the generation of dislocations at the tip of the crack did not occur and cycling of the associated peak stress values at the crack tip caused a relatively large plastic zone to form in front of the advancing

crack. This plastic zone with its high vacancy concentrations within the associated slip bands along with the formation of micro-cracks ahead of the crack tip would have allowed a fairly rapid diffusion of the corrosive species, believed to be sulphur in this case, that may ultimately have caused the change in fatigue mechanism. The precorrosion of the test specimens ensured that the corrosive elements had diffused sufficiently into the material and the fatigue testing was performed on corroded material.

Acknowledgements

The authors would like to acknowledge Siemens Industrial Turbomachinery Limited for the funding of the work.

References:

1. B. Bordenet: ‘High temperature corrosion in gas turbines: thermodynamic modelling and experimental results’, PhD thesis, RWTH Aachen University, Saarbrucken, Germany, 2004, 7-11.
2. H. Lai: ‘High temperature oxidation and corrosion of ni-based superalloys for industrial gas turbines’, PhD thesis, Chalmers University of Technology, Goteborg, Sweden, 2014, 2-19.
3. J. Sumner, A. Encinas-Oropesa, N. J. Simms and J. R. Nicholls: ‘Type II hot corrosion: behaviour of CMSX-4 and IN738LC as a function of corrosion environment’, *Materials and Corrosion*, 2014, **65**, (2), 188-196.
4. P. P. Milella: ‘Fatigue and corrosion in metals’ 1, 8-15, 2013, Milan, Springer (e-book, available at [http://www.springer.com/gp/book/9788847023352]).
5. G. E. Korth: ‘Effects of various parameters on the fatigue life of alloy 718, *TMS*, 1991, Superalloys 718, 625 and Various Derivatives, 457-476.
6. W. P. Wu and Z. Z. Yao: ‘Influence of a strain rate and temperature on the crack tip stress and microstructure evolution of monocrystalline nickel: a molecular dynamics simulation’, *Strength of Materials*, 2014, **46**, (2), 164-171.
7. H. J. Lim, B. Song, B. Park and H. Sohn: ‘Noncontact fatigue crack visualization using nonlinear ultrasonic modulation’, *NDT&E International*, 2015, **73**, 8-14.

8. C. E. Jaske, J. H. Payer and V. S. Balint: ‘Corrosion fatigue of metals in marine environments’, Report MCIC-81-42, Metals and Ceramics Information Center, Ohio, USA, 1981, 1-262.
9. A. Stockdale: ‘The corrosion and corrosion fatigue behaviour of nickel based alloy weld overlay and coextruded claddings’, PhD thesis, Lehigh University, Bethlehem, Pennsylvania, USA, 2014, 19-26.
10. S. Kawai and K. Koibuchi: ‘Effect of waveform on corrosion fatigue crack growth’, *Fatigue of Engineering Materials and Structures*, 1979, **1**, 395-407.
11. B. Ruttery, M. Ramsperger, L. Mujica Roncery, I. Lopez-Galilea, C. Korner and W. Theisen: ‘Impact of hot isostatic pressing on microstructure of CMSX-4 Ni-base superalloy fabricated by selective electron beam melting’, *Materials and Design*, 2016, **110**, 720-727.

List of figures and figure captions:

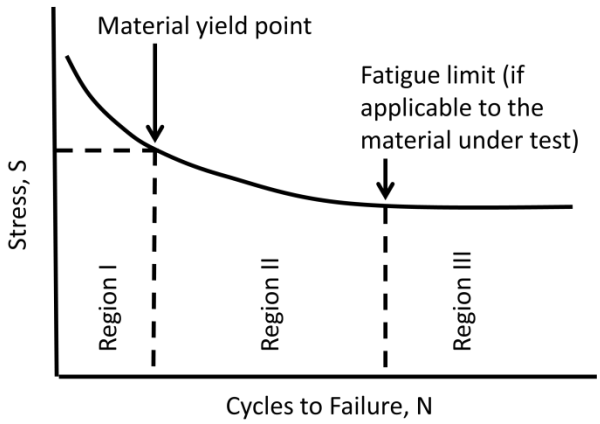


Figure 1: Example of S-N curve showing different regions

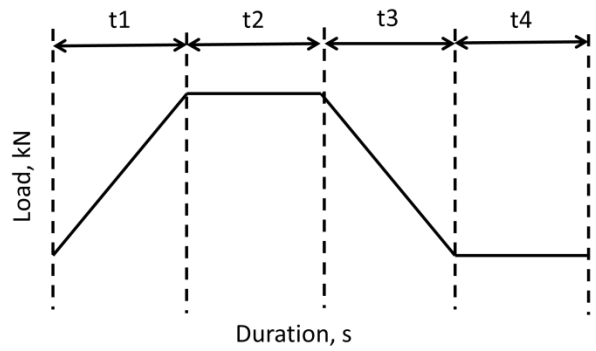


Figure 2: Various periods of the trapezoidal waveform, where in t1 the load increases, in t2 the maximum load is held, in t3 the load decreases and in t4 the minimum load is held. The trapezoidal waveform is written in the form: t1-t2-t3-t4

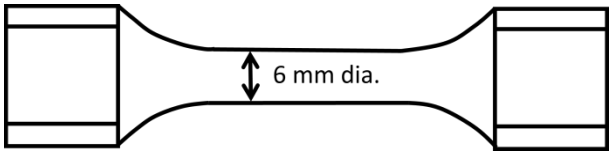


Figure 3: Schematic of plain fatigue test specimen

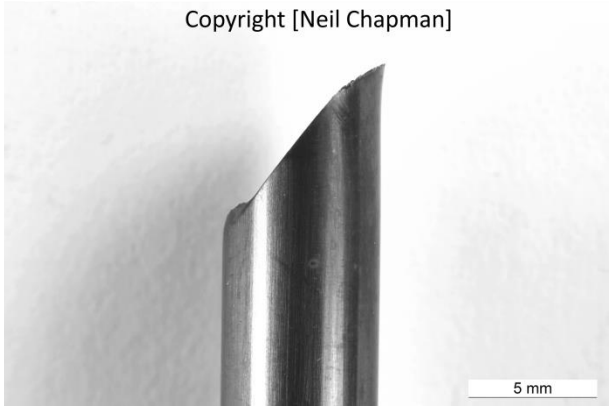


Figure 4: Low powered optical microscope image of fractured test specimen showing the typical 55° crack/fracture angle produced from fatigue testing in air using the 10-1-1-1 s waveform and non-precorroded test specimen

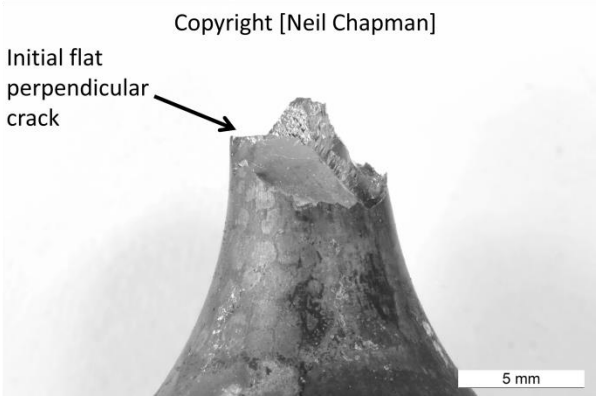


Figure 5: Low powered optical microscope image of fractured test specimen showing deviation from the typical 55° crack/fracture angle produced from corrosion fatigue testing using the 10-1-1-1 s waveform and non-precorroded test specimen

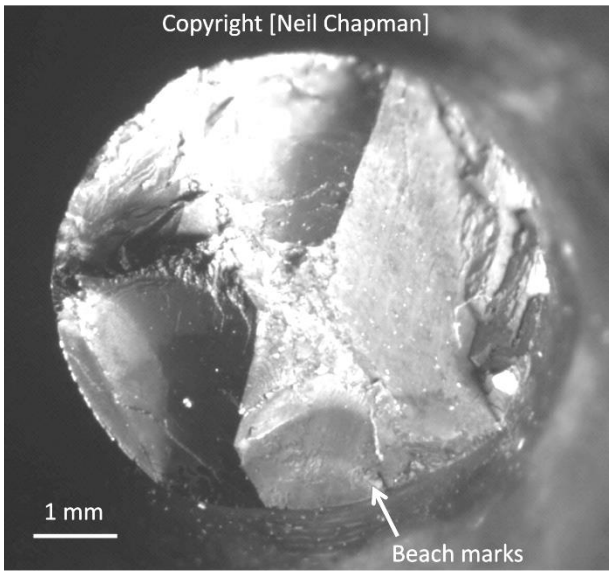


Figure 6: Low powered optical microscope image of beach marks observed on the initial flat perpendicular crack from the corrosion fatigue test using the 10-1-1-1 s waveform and non-precorroded test specimen

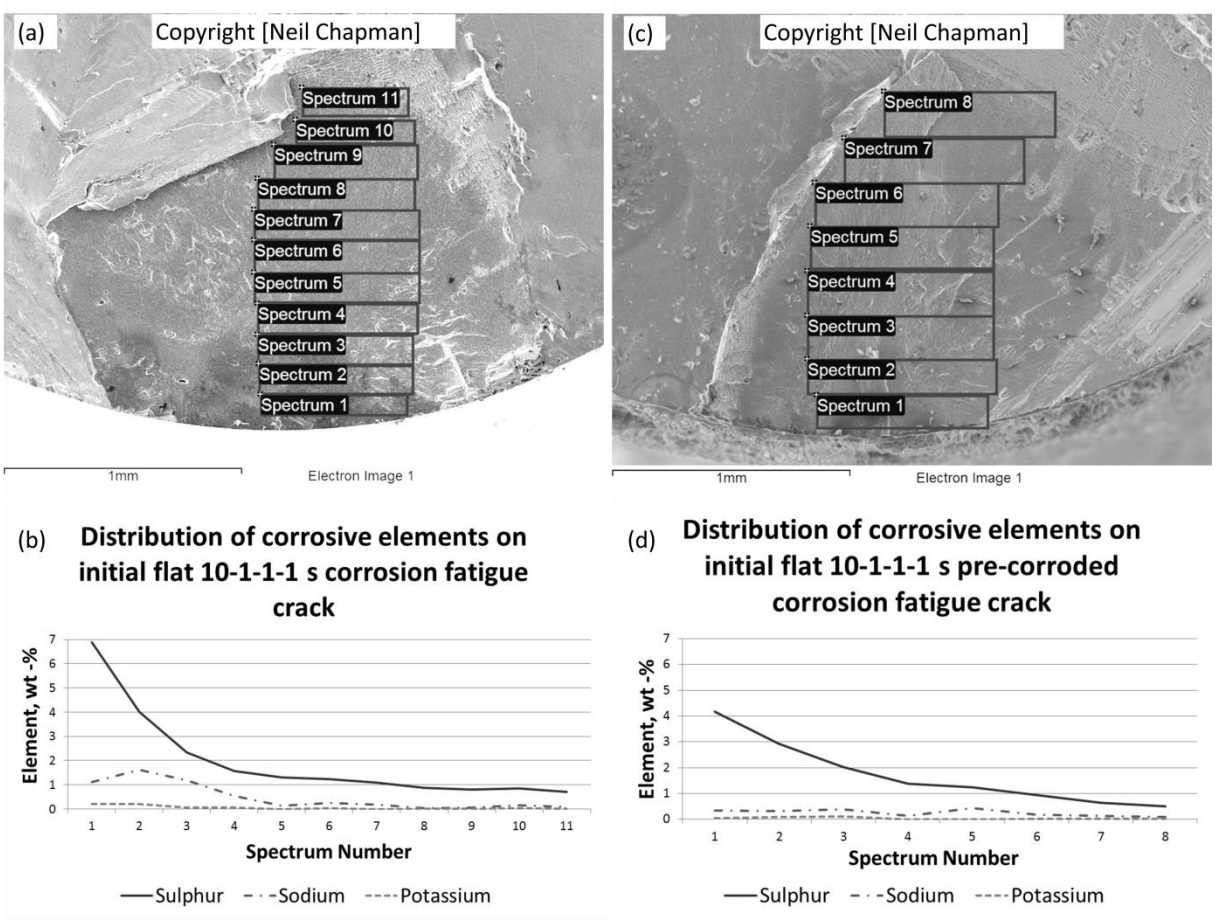


Figure 7: (a) SEM image showing locations of X-ray acquisition regions for EDX analysis line plots (b) obtained from the initial flat perpendicular crack from the corrosion fatigue test using the 10-1-1-1 s waveform and non-precorroded test specimen. (c) SEM image showing locations of X-ray acquisition regions for EDX analysis line plots (d) obtained from the initial flat perpendicular crack from the corrosion fatigue test using the 10-1-1-1 s waveform precorroded test specimen

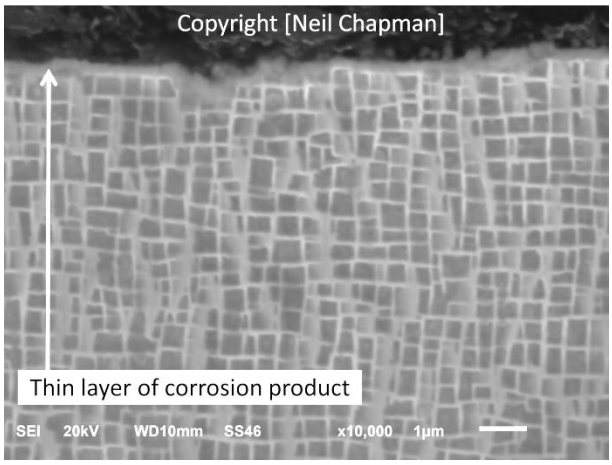


Figure 8: SEM image of microsection showing thin layer of corrosion product at mid crack position on the initial flat perpendicular crack from the corrosion fatigue test using the 10-1-1-1 s waveform and non-precorroded test specimen

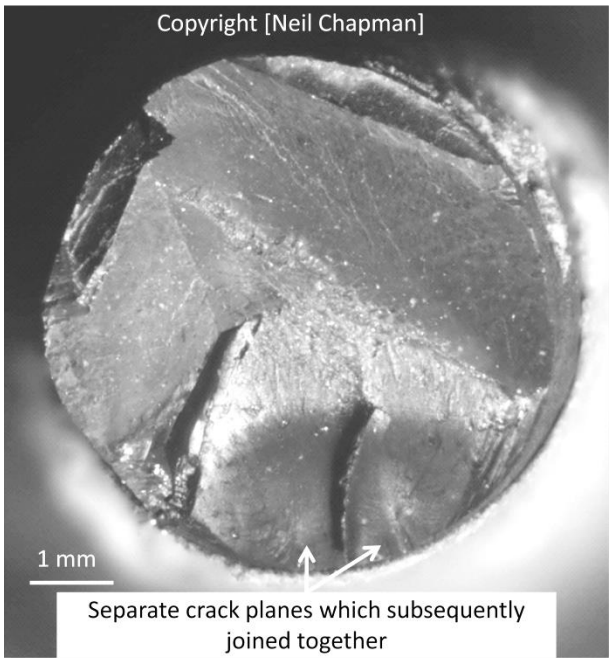


Figure 9: Low powered optical microscope image of two initial flat perpendicular cracks from the corrosion fatigue test using the 10-1-1-1 s waveform and precorroded test specimen

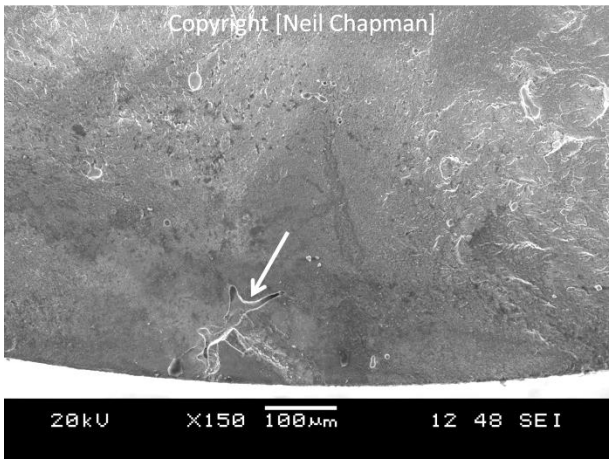


Figure 10: SEM image showing an example of an internal origin of the initial flat perpendicular corrosion fatigue crack (produced using the 10-1-1-1 s waveform and non-precorroded test specimen)

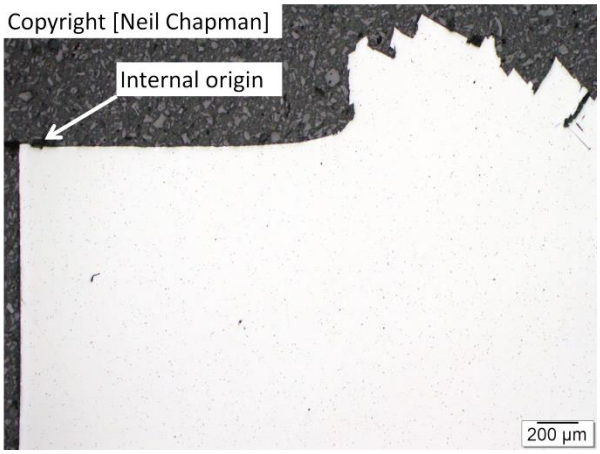


Figure 11: High powered optical microscope image of un-etched microsection showing an example of the initial flat perpendicular corrosion fatigue crack (produced using the 10-1-1-1 s waveform and non-precorroded test specimen)

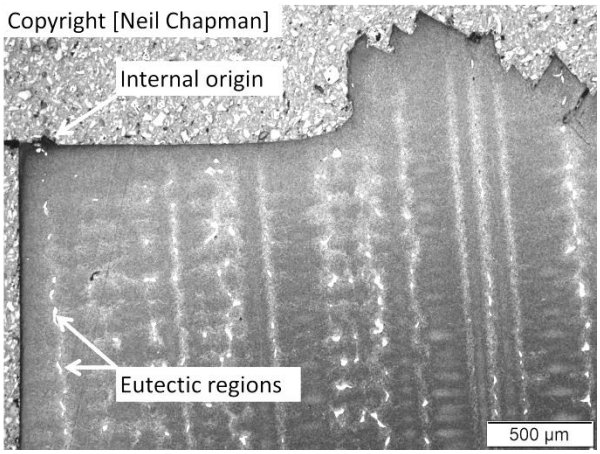


Figure 12: High powered optical microscope image of etched microsection showing an example of the initial flat perpendicular corrosion fatigue crack (produced using the 10-1-1-1 s waveform and non-precorroded test specimen)

List of tables and table figures:

Table 1 Chemical composition of CMSX-4 in weight percentage (wt-%)

Alloy	Ni	Cr	Co	Mo	W	Al	Ti	Ta	Hf	Re
Wt-%	61.7	6.5	9	0.6	6	5.6	1	6.5	0.1	3

Table 2 Test conditions for the fatigue tests conducted

Environment	Waveform parameters (s)	Precorroded test specimen	Number of re-salts required
Laboratory air	1-1-1-1	No	…
Corrosive	1-1-1-1	No	0
Corrosive	1-1-1-1	Yes	0
Laboratory air	10-1-1-1	No	…
Corrosive	10-1-1-1	No	1
Corrosive	10-1-1-1	Yes	0
Laboratory air	10-1-1-1	Yes	…
Corrosive	1-10-1-1	No	2

Table 3 Results of fatigue and corrosion fatigue tests

Environment	Waveform parameters (s)	Precorroded test specimen	Normalised cyclic data	Normalised hours data	Deviation of crack/fracture facets from 55° angle?
Laboratory air	1-1-1-1	No	1.0	1.0	No
Corrosive	1-1-1-1	No	1.4	1.4	No
Corrosive	1-1-1-1	Yes	0.9	0.9	Yes
Laboratory air	10-1-1-1	No	1.3	4.1	No
Corrosive	10-1-1-1	No	0.8	2.6	Yes
Corrosive	10-1-1-1	Yes	0.3	1.0	Yes
Laboratory air	10-1-1-1	Yes	1.6*	5.2*	…
Corrosive	1-10-1-1	No	1.6	5.2	No

Where:
* indicates test specimen did not fail and considered a runout

Normalised data is expressed as a factor of the Laboratory air 1-1-1-1 s test



https://dspace.org/

Corrosion fatigue testing: the combined effect of stress and high temperature corrosion

Chapman, Neil; Brooking, Laurie; Sumner, Joy; Gray, Simon; Nicholls, John R.

2017-10-20
Taylor & Francis
http://dx.doi.org/10.1080/09603409.2017.1389100
Chapman N, Brooking L, Sumner J, Gray S, Nicholls J, Corrosion fatigue testing: the combined effect of stress and high temperature corrosion, Materials at High Temperatures, Volume 35, 2018 - Issue 1-3: Microscopy of Oxidation 10, pp151-158

Downloaded from a DSpace repository. https://dspace.org/